How Kaposi's sarcoma-associated herpesvirus stably transforms peripheral B cells towards lymphomagenesis

Aurélia Faure[a], Mitch Hayes[a], and Bill Sugden[a,1]

[a]McArdle Laboratory for Cancer Research, University of Wisconsin–Madison, Madison, WI 53705

Edited by Thomas E. Shenk, Princeton University, Princeton, NJ, and approved July 3, 2019 (received for review March 23, 2019)

Primary effusion lymphomas (PELs) are causally associated with Kaposi's sarcoma-associated herpesvirus (KSHV) and 86% of PELs are coinfected with Epstein–Barr virus (EBV). Understanding how PELs develop has been impaired by the difficulty of infecting B cells with KSHV in vitro, and the inability of KSHV to transform them. We show that EBV supports an optimal coinfection of 2.5% of peripheral B cells by KSHV. This coinfection requires 1 or more transforming genes of EBV but not entry into KSHV's lytic cycle. We demonstrate that dually infected B cells are stably transformed in vitro and show that while both viruses can be maintained, different cells exhibit distinct, transformed properties. Transformed cells that grow to predominate in a culture express increased levels of most KSHV genes and differentially express a subset of cellular genes, as do bona fide PEL cells. These dually infected peripheral B cells are thus both stably transformed and allow in vitro molecular dissection of early steps in the progression to lymphomagenesis.

primary effusion lymphoma | KSHV | EBV | in vitro transformation

Primary effusion lymphoma (PEL) is a highly aggressive form of non-Hodgkin's lymphoma found primarily in HIV-infected patients (1). PEL presents as lymphomatous effusions that grow mainly in the body cavities. The prognosis for patients is poor, with a median survival of about 6 mo postdiagnosis (1, 2). PELs are causally associated with Kaposi's sarcoma-associated herpesvirus (KSHV), and 86% of them are also coinfected with Epstein–Barr virus (EBV) (1, 3). EBV and KSHV (also known as human herpesviruses 4 and 8 [HHV-4 and HHV-8]) are 2 related oncogenic human γ-herpesviruses. They can persist latently in host cells, expressing a limited set of viral genes while maintaining their genomes as extrachromosomal plasmids. The maintenance of KSHV and EBV genomes as plasmids in PELs indicates that both viruses contribute to tumor phenotypes: these viral genomes are lost from proliferating cells if they do not provide their host cells some selective advantages (4–6). The KSHV genome is retained as a plasmid both in PEL cells in vivo and upon explantation in vitro. In addition, several KSHV genes have been shown to be essential for the survival or proliferation of these cells (7–9). KSHV is therefore thought to be the genetic driver for PEL.

We formerly lacked a model that allows complete characterization in vitro of the early steps of development of PEL: B cells have been notoriously difficult to infect with KSHV in vitro and when they can be infected, KSHV has not been found to transform them. The difficulty to infect B cells with KSHV in vitro was unexpected given its detection in B cell fractions in vivo. Even though KSHV causes Kaposi's sarcoma (KS) where it infects endothelial cells (10–13), KSHV viral DNA has been detected in populations of circulating B cells in vivo in both healthy individuals and KS patients (14–16). In addition to PEL, KSHV has also been associated with multicentric Castleman's disease, a nonmalignant lymphoproliferative disorder (17). While cells of endothelial and fibroblast origin can be efficiently infected with KSHV in vitro, attempts to infect lymphoblastic cell lines including B and T cell lines have been unsuccessful (18–21). In these studies, neither EBV^- nor EBV^+ B cell lines could be infected. Several studies have found that primary $CD19^+$ B cells isolated from peripheral blood and umbilical cord blood mononuclear cells are susceptible to KSHV infection (19, 21, 22). However, KSHV did not lead to transformation of these cells and infection could only be detected by DNA PCR or RT-PCR shortly after infection. Recently, several groups have reported more robust infection of primary B cells isolated from tonsils with 0.5 to 10% of tonsillar B cells being infected with KSHV (23–27). In this instance, KSHV infection could only be studied in these cells for short periods of time because of KSHV's apparent inability to transform them (24, 26, 27).

Therefore, the conditions necessary for KSHV to infect B cells that lead to PEL remain unclear. We reasoned that because EBV is also found as a plasmid in the majority of examined PELs, it would be providing these cells one or more selective advantages. In contrast to KSHV, EBV can infect and transform peripheral B cells in vitro and induce their long-term proliferation (28, 29). One study has reported detection of KSHV DNA by PCR in newly transformed B cells following exposure to both viruses, suggesting that cells can be dually infected in vitro (21). In addition, a recent study found that KSHV was detected more often in the spleen and blood of NSG mice reconstituted with human $CD34^+$ cells when these mice were infected with KSHV and EBV compared with KSHV alone (30). Here we describe extensive, quantitative experiments in which we define a role for EBV in supporting coinfection by KSHV. We show that EBV promotes infection of peripheral B cells with KSHV, and that this efficiency of infection is optimal within 24 h of EBV infection. We characterized the dually infected, proliferating B

Significance

Primary effusion lymphoma (PEL) is a highly aggressive B cell lymphoma. PELs are associated with Kaposi's sarcoma-associated herpesvirus (KSHV), and most of them are coinfected with Epstein–Barr virus (EBV). Human B cells have not previously been stably infected with KSHV in vitro. In this study, we have defined conditions to infect human B cells stably with KSHV and show that optimal infection requires coinfection by EBV. We show that a subset of these dually infected cells acquires multiple properties of PEL cells. This dual infection in vitro allows a mechanistic analysis of the contributions of EBV and KSHV to early steps in the development of PEL and underscores the desirability of targeting both viruses in developing new therapies for PEL.

Author contributions: A.F., M.H., and B.S. designed research, performed research, analyzed data, and wrote the paper.

The authors declare no conflict of interest.

This article is a PNAS Direct Submission.

Data deposition: The data reported in this paper have been deposited in the NCBI Sequence Read Archive (BioProject accession no. PRJNA544266).

[1]To whom correspondence may be addressed. Email: sugden@oncology.wisc.edu.

This article contains supporting information online at www.pnas.org/lookup/suppl/doi:10.1073/pnas.1905025116/-/DCSupplemental.

Published online July 30, 2019.

cells: they were transformed, maintaining both KSHV and EBV for months in culture. Some transformed cells grew more slowly than cells infected only with EBV and were often overgrown, whereas others grew to dominate the culture. These latter cells showed increased expression of most KSHV genes, including those encoded by the latency locus, regulated the expression of some cellular genes as do PEL cells, and thus shared multiple properties with PEL cells. This in vitro transformation of peripheral B cells by KSHV and EBV allows a mechanistic analysis of the viral and cellular genes that mediate early events in the progression toward PEL.

Results

In Vitro Activation of Peripheral B Cells Supports Detectable but Inefficient KSHV Infection. Peripheral blood mononuclear cells (PBMCs) were isolated from blood and $CD19^+$ B cells were purified from them by negative selection to avoid stimulation of cell surface receptors. These $CD19^+$ B cells were exposed to concentrated viral stocks of KSHV BAC16 using a multiplicity of infection (MOI) of 2 to 3 as determined on 293 cells. KSHV BAC16 is derived from the rKSHV.219 virus, isolated from the JSC-1 PEL cell line (31). The recombinant KSHV BAC16 virus contains a GFP reporter driven by the constitutively active promoter EF1α. Previous studies (24) and our own observations showed that, even following extensive washes, KSHV viral particles remain bound to the surface of primary B cells. Therefore, GFP expression allowed us to monitor successful KSHV infection, as opposed to nucleic acid detection that does not distinguish viral entry from cell surface-bound particles. In addition, we confirmed that GFP expression indicates the presence of KSHV DNA in cells as measured by FISH (see below).

We found that peripheral B cells were refractory to infection by KSHV. Peripheral $CD19^+$ B cells were spinoculated with KSHV BAC16 virus, before washing to remove unbound virus and subsequently cultured for 4 to 7 d to allow GFP expression. We monitored the number of $CD19^+$ B cells expressing GFP by flow cytometry and detected no KSHV-infected (GFP^+) $CD19^+$ B cells in 5 independent biological replicates obtained from 3 different blood donors (Fig. 1). Furthermore, no GFP^+ cells were detected by fluorescence microscopy at day 1, 2, or 3, confirming that no detectable KSHV infection occurred before flow cytometry. These results demonstrate that KSHV cannot establish successful infection in resting, peripheral $CD19^+$ B cells.

Because researchers have reported successful infection of tonsillar B cells, which often contain activated B cells, we tested whether B cell activation supports detectable KSHV infection. Isolated $CD19^+$ B cells were exposed to KSHV BAC16 at different time points before or following activation with IL-4 and CD40L. We found that in vitro activation of peripheral B cells could support, in some cases, detectable but inefficient KSHV infection (Fig. 1). Infection of peripheral B cells with KSHV was highest when cells were infected with KSHV before IL-4 and CD40L activation ($0.13 \pm 0.14\%$ with a maximum of 0.28% of GFP^+ cells). In comparison, $0.02 \pm 0.02\%$, $0.03 \pm 0.01\%$, and $0.06 \pm 0.06\%$ of B cells were GFP^+ when cells were exposed to KSHV, respectively, on days 0, 1, and 3 following B cell activation. These low efficiencies in the presence of IL-4 and CD40L were confirmed as live cells were passaged for ∼5 doublings and GFP^+ cells could still be detected by flow cytometry. While an earlier study (32) reported up to 30% of activated peripheral B cells to be susceptible to infection, although we infected similarly activated, peripheral B cells from multiple donors in 10 separate experiments, we found no more than 0.13% of them to be infected with KSHV (Fig. 1).

EBV Infection Supports an Optimal Infection of Peripheral B Cells by KSHV. We tested whether EBV coinfection supports an optimal infection of peripheral B cells with KSHV. Peripheral $CD19^+$ B cells were infected with the B95-8 strain of EBV at an MOI of 1 to 2. An average of 70% of the cells were blasts at day 3 or 4 postinfection with EBV (average from 7 independent biological replicates). $CD19^+$ B cells were exposed to KSHV

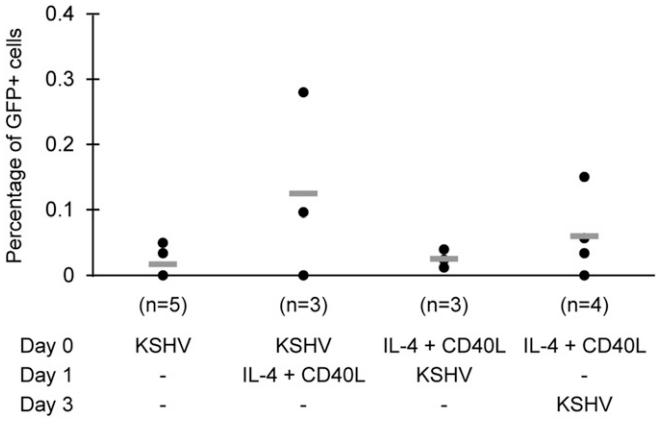

Fig. 1. IL-4 and CD40L activation of peripheral B cells supports detectable but inefficient KSHV infection. Isolated $CD19^+$ B cells were exposed to KSHV BAC16 at an MOI of 2 to 3 by spinoculation at different time points following or before activation with IL-4 and CD40L. In all conditions, cells were cultured for 4 to 7 d following exposure to KSHV. Live cells were analyzed for CD19 and GFP expression using a BD LSR Fortessa cytometer, and analysis was performed using FlowJo software. Each dot represents the percentage of GFP^+ cells measured in one biological replicate. The number of biological replicates is indicated for each condition. The mean of data are indicated by the horizontal bar. $P > 0.05$ between each condition by Wilcoxon rank sum test.

BAC16 at different time points before, on the same day as, or following EBV infection. EBV infection promoted optimal infection (up to a 20-fold increase relative to activated B cells) of peripheral B cells with KSHV (up to $2.50 \pm 1.13\%$) (Fig. 2 *A* and *B*). The efficiency of infection with KSHV was comparable to that previously reported in tonsillar B cells (23–27). However, EBV played a conflicting role in KSHV infection: early events of EBV infection promoted infection by KSHV but later events inhibited this coinfection. We found that infection of peripheral B cells with KSHV was highest when cells were exposed to KSHV 1 d before EBV infection ($2.50 \pm 1.13\%$ with a maximum of 3.53% of GFP^+ cells). This efficiency decreased rapidly following infection with EBV, declining to $0.64 \pm 0.45\%$ with KSHV infection at day 1 and to $0.10 \pm 0.05\%$ at day 3 post-EBV infection. These measurements are consistent with reports of EBV^+ B cell lines being resistant to KSHV infection (19–21). When cells were exposed to the 2 viruses on the same day the efficiency of infection with KSHV was $1.11 \pm 0.33\%$. Therefore, optimal infection of peripheral B cells with KSHV is achieved when cells are exposed to KSHV within 24 h of EBV infection. We achieved this optimal coinfection using spinoculation to infect B cells with KSHV because it yielded a comparable or higher level of infection than did cocultivation of tonsillar B cells (23), and it allowed us to measure the number of infectious particles required for successful, dual infections.

We examined what EBV contributes to foster KSHV infection. First, does EBV induce a potential KSHV entry receptor? DC-SIGN, also called CD209, was reported to be a receptor for KSHV entry in peripheral $CD19^+$ B cells (32) and is the only potential receptor for KSHV previously described to be on B lymphocytes (33, 34). We used 2 different anti–DC-SIGN antibodies and validated them on the human monocytic THP-1 cell line (35, 36) (*SI Appendix*, Fig. S1*A*). No expression of DC-SIGN on either uninfected B cells or EBV-infected B cells at 1 d postinfection was detectable (*SI Appendix*, Fig. S1*B*). Similar results were obtained with the second anti–DC-SIGN antibody on uninfected B cells or EBV-infected B cells at 4 d postinfection. These results indicate that DC-SIGN is not required for KSHV entry into B cells.

Second, we tested whether EBV is necessary for KSHV entry into B cells. We determined if KSHV infection could be blocked with a neutralizing antibody against KSHV glycoprotein gpK8.1A (anti-gpK8.1A 4A4) immediately before infection with EBV.

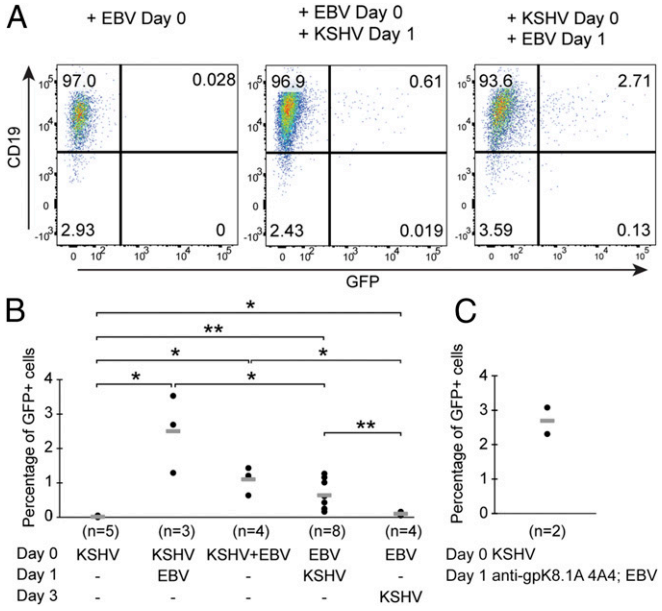

Fig. 2. EBV infection supports an optimal infection of peripheral B cells by KSHV. (*A* and *B*) Isolated CD19$^+$ B cells were exposed to KSHV BAC16 at an MOI of 2 to 3 by spinoculation at different time points following, before, or on the same day as EBV infection. (*C*) Isolated CD19$^+$ B cells were exposed to KSHV BAC16 at an MOI of 2 by spinoculation. Cells were washed to remove excess, unbound virus and treated 24 h later with anti-gpK8.1A 4A4 for 2 h at 37 °C. Cells were then washed and infected with EBV. In all conditions, cells were cultured for 4 to 7 d following exposure to KSHV. Live cells were analyzed for CD19 and GFP expression using a BD LSR Fortessa cytometer, and analysis was performed using FlowJo software. (*A*) One representative experiment is shown out of 3 to 8 independent biological replicates. (*B* and *C*) Each dot represents the percentage of GFP$^+$ cells measured in 1 biological replicate. The number of biological replicates is indicated for each condition. The mean of data are indicated by the horizontal bar. *$P < 0.05$; **$P < 0.01$ by Wilcoxon rank sum test.

Virion envelope-associated gpK8.1A is thought to mediate KSHV binding to target cells via interaction with heparan sulfate moieties (37). Studies have indicated that the gpK8.1A glycoprotein is involved in KSHV binding to target cells but is not required for viral entry (38, 39). The anti-gpK8.1A 4A4 antibody inhibited infection by KSHV by 40 to 70% in 293 cells (*SI Appendix*, Table S1). CD19$^+$ B cells were treated with anti-gpK8.1A 4A4 24 h following exposure to KSHV and immediately before infection with EBV. The percentage of CD19$^+$ B cells infected was the same whether treated or not with the neutralizing antibody (Fig. 2*C*), indicating that KSHV virions became inaccessible to the neutralizing antibody before EBV infection either by entry into B cells or irreversible adsorption onto them. Therefore, KSHV either can enter nonactivated peripheral B cells or bind them irreversibly but cannot establish infection in the absence of EBV infection or B cell activation, which is also provided by EBV. We could not detect GFP expression in nonactivated peripheral B cells following exposure to KSHV, indicating that, if KSHV enters nonactivated B cells, B cell activation, or blast-formation is needed for KSHV gene expression. Importantly, and contrary to infections with EBV, exposure to KSHV alone did not induce proliferation and did not rescue nonactivated B cells from cell death.

Third, we tested which genetic contributions EBV makes to the early phase of dual infection by KSHV. Herpesviruses, such as human cytomegalovirus, carry viral proteins and mRNAs in virus particles that can contribute to the early stages of infection (40). EBV specifically carries mRNAs encoding BZLF1 (41), which is known to affect the early stages of infection. We used both γ-irradiation and an EBV mutant to characterize EBV's support of infection by KSHV. γ-Rays inhibit gene expression primarily by introducing double-stranded breaks into DNA. We used doses of γ-rays to irradiate a stock of B95-8 that would not inactivate proteins and mRNAs (42), coinfected B cells isolated from 2 donors along with KSHV, and measured the fraction of dually infected, GFP$^+$ cells. γ-Irradiation inhibited EBV's support of dual infection by KSHV dose-dependently (Table 1), showing that viral mRNAs and proteins in the virus particle are insufficient for dual infection by KSHV. The slope of this inhibition curve paralleled one we had found to inhibit expression of EBV's nuclear antigens early after infection (42). This requirement for EBV's nuclear antigens was tested with the EBNA2-null variant, HH514 clone 16 (43, 44), in dual infections and yielded a 62% decrease in GFP$^+$ cells relative to B95-8 virus at day 5 postinfection (Table 1). EBV, therefore, must express 1 or more transforming genes, including EBNA2, in primary B cells for dual infection and transformation by KSHV.

KSHV Lytic Gene Expression Is Not Required for Infection of Peripheral B Cells. We also tested for any required role for KSHV's lytic cycle in infection of peripheral B cells. Some groups reported latent KSHV infection (24), while others found high rates of spontaneous activation of the lytic cycle (25) during the first 5 d following infection of tonsillar B cells. We used a strain of KSHV, KSHV BAC16RTAstop, that does not express the viral protein RTA (45), which is required for entry into the lytic cycle. Cells infected with this strain of KSHV therefore cannot undergo the lytic cycle. We confirmed that the RTA gene was mutated in this strain of KSHV (*SI Appendix*, Fig. S2*A*). Isolated CD19$^+$ B cells were exposed to KSHV BAC16RTAstop at different time points before or following EBV infection or activation with IL-4 and CD40L. The mutant strain of KSHV infected peripheral B cells with similar efficiencies as the wild-type KSHV BAC16 strain (*SI Appendix*, Fig. S2*B*). Thus, KSHV lytic gene expression is not required for optimal infection of peripheral B cells.

Dually Infected, Proliferating B Cells Are Transformed to Maintain both Viruses. B cells have not yet been dually infected in vitro and propagated successfully over long times in culture. GFP$^+$ cells were therefore sorted from populations of cells exposed to

Table 1. EBV's nuclear antigens are required early for dual infection of peripheral B cells by KSHV

	Percent of support of KSHV infection			
	B95-8, %	B95-8 (3×10^4 rads), %	B95-8 (10×10^4 rads), %	HH514, %
Biological replicate 1	100	82	52	21
Biological replicate 2	100	70	58	55
Average	100	76	55	38

Peripheral B cells were exposed to KSHV and the wild-type B95-8 strain of EBV, the B95-8 strain of EBV following γ-irradiation, or the HH514 clone 16 strain of EBV. Cells were exposed to KSHV and EBV on the same day. The percentage of cells infected with KSHV was measured by flow cytometry in 2 independent biological experiments on day 5 postinfection.

both EBV and KSHV 3 to 7 wk postinfection. FACS-sorting initially yielded 60 to 90% GFP$^+$ cells. Subsequently, the fraction of GFP$^+$ cells in these sorted populations was monitored over time by fluorescence microscopy. In some populations, the fraction of GFP$^+$ cells decreased over time (Fig. 3*A*) and correlated with the fraction of cells positive for KSHV by FISH (Fig. 3*B*). The fraction of KSHV-infected and EBV-infected cells was monitored over time by FISH in both GFP$^-$ and GFP$^+$ populations (Fig. 3 *C*–*F*). In KSHV$^+$ cells, the copy number of KSHV genomes ranged from 2 to 28, with an average of 11 genomes per cell indicating that KSHV is extrachromosomal in these cells. In addition, GFP$^-$ populations were negative for KSHV by FISH, confirming that GFP was not silenced but that loss of GFP indicated either a decrease in the fraction of dually infected cells or a loss of KSHV genomes from dually infected cells in these populations. Most GFP$^-$ and GFP$^+$ cells were positive for EBV by FISH demonstrating that KSHV-infected cells were also infected with EBV. EBV$^+$ cells were maintained in both GFP$^-$ and GFP$^+$ cells over time and the number of EBV genomes ranged from 1 to 44 in these cells.

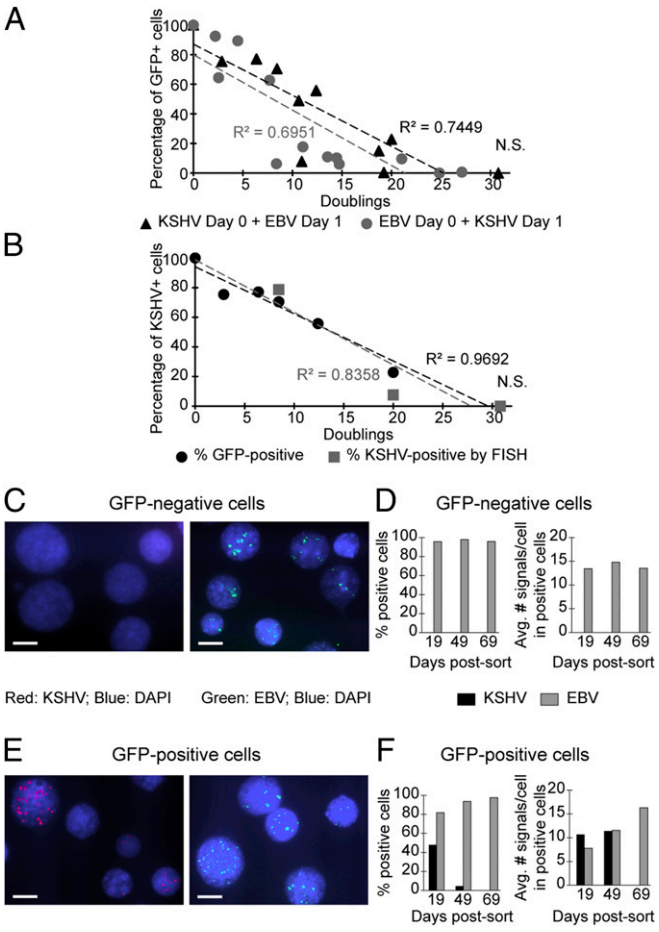

Fig. 3. The fraction of KSHV$^+$ cells decreases in some populations of infected peripheral B cells. Isolated CD19$^+$ B cells were exposed to KSHV 24 h before or following EBV infection. KSHV infected GFP$^+$ cells were sorted 3 to 7 wk postinfection. (*A*) The number of GFP$^+$ cells was monitored over time by fluorescence microscopy. The percentage of GFP$^+$ cells was normalized to the number of GFP$^+$ cells at zero doublings (first day after sorting). Data from 3 independent biological experiments are shown for each population. (*B*) The number of KSHV-infected cells was quantified by FISH and compared with the number of GFP$^+$ cells at 3 different time points in 1 experiment. The R^2 of the trendlines is indicated. N.S. $P > 0.05$ by Sen–Adichie test. (*C*–*F*) The number of KSHV- and EBV-infected cells was quantified over time by FISH in both GFP$^-$ and GFP$^+$ cells. (*C* and *E*) Representative FISH images are shown when samples were incubated with hybridization probes for detection of KSHV (*Left*) or EBV (*Right*) plasmids (Scale bars, 10 μm). (*D* and *F*) The percentage of EBV$^+$ and KSHV$^+$ cells and the average number of signals per cell in positive cells was determined by FISH at different time points following sorting.

Among these populations of infected B cells, some GFP$^+$, KSHV$^+$ cells began to predominate. We observed multiple fluctuations in the percentage of GFP$^+$ cells over time. Some populations, in which the percentage of GFP$^+$ cells had previously decreased, still maintained a low number of GFP$^+$ cells for several months. In others, the percentage of GFP$^+$ cells spontaneously increased in the absence of any selection by FACS, and either continued to increase over time or later decreased. We therefore tested whether the dually infected cells in populations of infected B cells were transformed to maintain both KSHV and EBV stably. We followed and repeatedly sorted 2 populations of infected cells obtained from 2 different blood donors for GFP, measured the number of EBV and KSHV genomes in them, and analyzed their proliferation and clonal composition based on VDJ recombination in the Ig heavy-chain locus. In the first population (population 1), the GFP$^+$ cells outgrew the GFP$^-$ cells to become stably, dually infected (we term these cells "KSHV$^+$/EBV$^+$-fast"). The percentage of GFP$^+$ cells increased from 1.4 to 90% over 5.5 mo and KSHV was still maintained in these cells after 7 mo of culture (Fig. 4*A*). We cultured and sorted portions of population 1 and compared their phenotypes to those of a second population (population 2) that needed FACS selection of the GFP$^+$ fraction (termed "KSHV$^+$/EBV$^+$-slow") to avoid its being overgrown. Early in the culturing of this second population (before FACS selection), the percentage of dually infected, GFP$^+$ cells increased to ∼10% before the GFP$^-$ cells (EBV-only infected cells) began to overgrow them. These 2 populations were compared longitudinally for 3 to 5 mo.

Cells from unsorted and sorted populations were collected at different time points and analyzed for the presence of KSHV and EBV by qPCR (Fig. 4*B*). The average number of KSHV genomes per cell in the population 1 increased over time from ∼3 to 31 genomes per cell. Analysis by FISH showed that this increase is due to the percentage of KSHV$^+$ cells (KSHV$^+$/EBV$^+$-fast cells) increasing over time in the population and reaching almost 100%, while the average number of KSHV genomes remained constant in these cells (*SI Appendix*, Fig. S3). In population 2, there were on average ∼6 KSHV genomes per cell by qPCR, which correlated with a low fraction of cells being KSHV$^+$ (KSHV$^+$/EBV$^+$-slow cells) at the time of analysis. Analysis by FISH indicated that the average number of KSHV genomes per cell in the KSHV$^+$/EBV$^+$ fast and the KSHV$^+$/EBV$^+$ slow cells was similar (between 11 and 16 genomes per cell) and that KSHV was present as a plasmid in these cells (with a range of 1 to 52 and 1 to 27 KSHV signals per cell, respectively) (*SI Appendix*, Fig. S3). Furthermore, analysis by FISH confirmed that the KSHV$^+$/EBV$^+$-fast cells were not overgrown by KSHV$^-$ cells: close to 100% of the cells remained KSHV$^+$ following each sort, as opposed to the KSHV$^+$/EBV$^+$ slow cells that were overgrown by the EBV-only infected cells (only ∼35% of the cells were KSHV$^+$ 31 d after sort). The average number of EBV genomes per cell was similar in population 1 (∼11 to 33 genomes per cell) and population 2 (∼10 genomes per cell).

To look for competitive growth advantages between dually infected and EBV-only infected cells, we analyzed the clonal composition of populations 1 and 2. RNA was isolated at different time points before and after sorting of GFP$^+$ cells RNA-sequencing (RNA-seq) was performed (46) and analyzed computationally with MiXCR, to determine the percentage of each clone based on VDJ recombination in the Ig heavy-chain locus (Fig. 5). In the first population, the dually infected GFP$^+$ cells (KSHV$^+$/EBV$^+$-fast cells) represented primarily 1 clone that overgrew other cells in the population and was also selected by sorting the GFP$^+$ cells. Analysis with MiXCR indicated that this clone expressed IgM and λ-light chain mRNA (*SI Appendix*, Table S2). Interestingly, in the second population, dually infected KSHV$^+$/EBV$^+$-slow cells were likely also clonal because a clone and its progeny, also expressing IgM and λ-light chain mRNA, predominated after each sort of GFP$^+$ cells. However, contrary to the KSHV$^+$/EBV$^+$-fast cells, these cells were overgrown

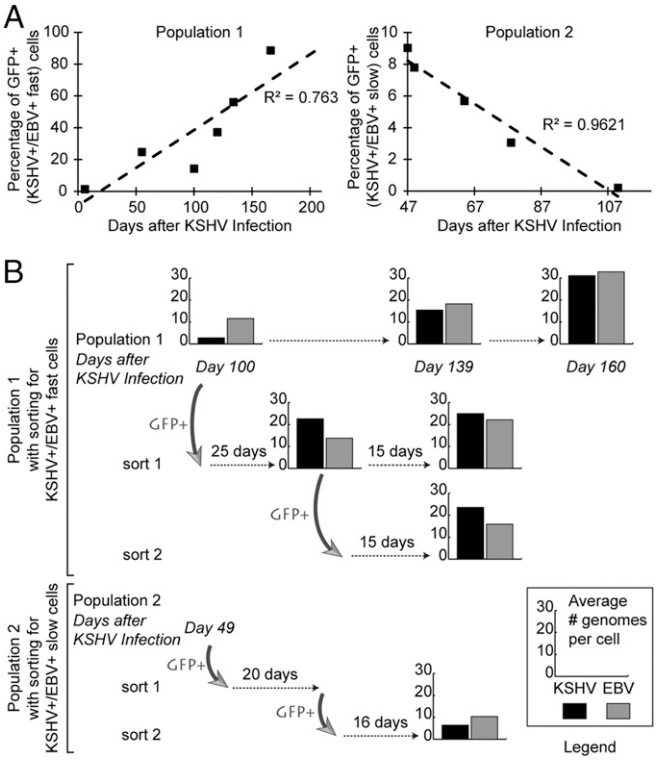

Fig. 4. Some cells within populations of infected B cells maintain both viruses. (*A*) Following KSHV infection, the percentage of GFP$^+$ cells was followed over time in the populations 1 and 2. Live cells were analyzed for GFP expression using a BD LSR Fortessa cytometer, and analysis was performed using FlowJo software. (*B*) Populations shown in *A* were repeatedly sorted for GFP$^+$ cells (KSHV$^+$/EBV$^+$-fast and KSHV$^+$/EBV$^+$-slow cells, respectively) (gray arrows) and harvested in TRIzol at different time points. Following isolation of DNA, the average number of EBV and KSHV genomes per cell was quantified by qPCR.

by other clones. The EBV-only infected clones that overgrew the KSHV$^+$/EBV$^+$-slow cells expressed IgM or IgG and κ–light-chain mRNA as shown by the increase in IgG and κ-light chain expression when cells were left unsorted (*SI Appendix*, Table S2). These findings indicate that the KSHV$^-$ cells that overgrew the sorted dually infected, GFP$^+$ cells usually arose from preexisting KSHV$^-$, EBV-only infected cells, which contaminated the FACS sorts. Therefore, both the KSHV$^+$/EBV$^+$-fast and the KSHV$^+$/EBV$^+$-slow cells were transformed to maintain KSHV and EBV stably over time, but the KSHV$^+$/EBV$^+$-fast cells had a proliferative advantage over the EBV-only infected cells as opposed to the KSHV$^+$/EBV$^+$-slow cells.

We measured the frequency with which dually infected B cells yielded stably transformed progeny. B cells from 2 donors were purified and exposed to both viruses. For both donors the cells were sorted at day 7 postinfection; for 1 donor an aliquot was also sorted at day 12. Sorted, GFP$^+$ cells were plated on human fibroblast feeders using 2-fold dilutions, each with 8 replicates, and followed for 7 to 8 wk. Cloning efficiencies were determined from Poisson statistics for all 3 end-point dilutions. On average, 2% of B cells exposed to both viruses yielded GFP$^+$, dually infected cells on day 7. When these cells were serially diluted, on average, 5% of the wells having 1 cell or less formed stably proliferating populations, of which 40% remained GFP$^+$, thus dually infected. We defined the KSHV$^+$/EBV$^+$-fast transformed cells as dually infected cells which overgrew mixed populations such that all cells grew to be GFP$^+$. To understand the frequency at which KSHV$^+$/EBV$^+$-fast cells arise, we looked at wells in which multiple cells capable of proliferating were plated and counted only those wells at 7 wk in which all cells were GFP$^+$. The frequency of such cells in initially mixed populations was found to be 10%. The KSHV$^+$/EBV$^+$-fast transformed cells thus comprised ∼1 cell per 10,000 (0.02 × 0.05 × 0.1) B cells exposed to both KSHV and EBV.

KSHV Gene Expression Is Increased in the KSHV$^+$/EBV$^+$-Fast Transformed Cells. We analyzed the viral and cellular mRNAs expressed in populations 1 and 2. We analyzed enriched fractions of dually infected cells (≥60% GFP$^+$) that spontaneously arose in the population or were obtained by FACS selection, as shown in Fig. 5. We isolated RNA sequentially over a period of 3 to 5 mo from 7 samples of KSHV$^+$/EBV$^+$-fast cells (population 1) and 5 samples of KSHV$^+$/EBV$^+$-slow cells (population 2). The viral RNAs were mapped to their respective genomes following the approach of Bruce et al. (47) to disentangle any overlapping transcripts.

More than 6,000 cellular genes, some EBV genes (17 of 78) and most KSHV genes (72 of 98) were differentially expressed between the KSHV$^+$/EBV$^+$-fast and the KSHV$^+$/EBV$^+$-slow transformed cells (Fig. 6*A*). Differentially expressed EBV and KSHV genes were mainly up-regulated in the KSHV$^+$/EBV$^+$-fast cells compared with the KSHV$^+$/EBV$^+$-slow cells and are represented in Fig. 6 *B* and *C*. The levels of EBV nuclear antigens and of LMP1, however, did not differ significantly between the 2 cell populations. Among the 72 up-regulated KSHV genes, most of the latency locus genes (48) were statistically up-regulated in the KSHV$^+$/EBV$^+$-fast cells compared with the KSHV$^+$/EBV$^+$-slow cells, including v-FLIP (ORF71), v-cyclin (ORF72), LANA1 (ORF73), Kaposin A/C (ORF K12), and the miRNA cluster (miR region). In addition, expression of vIL-6 (ORF K2), which is thought to serve as a growth factor for PEL (49, 50), was increased in the KSHV$^+$/EBV$^+$-fast cells by ∼250-fold. Coverage plots of RNA-seq reads also showed the increased KSHV gene expression in the KSHV$^+$/EBV$^+$-fast cells compared with the KSHV$^+$/EBV$^+$-slow

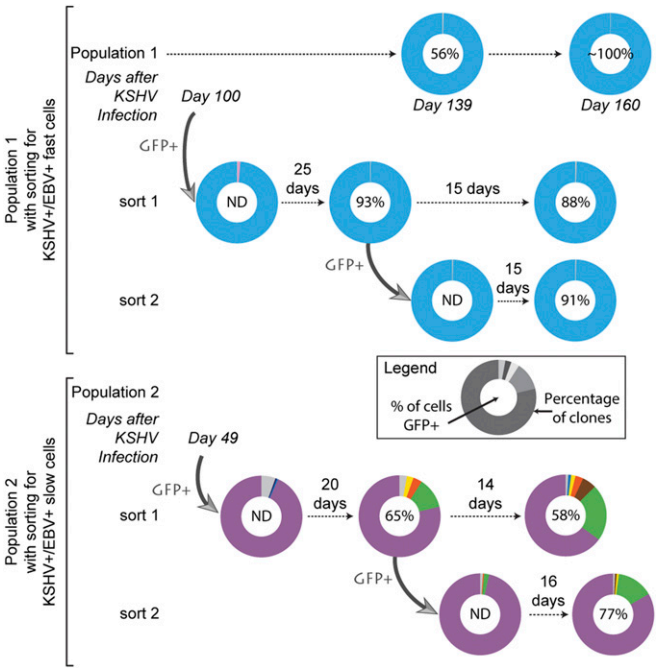

Fig. 5. KSHV$^-$ cells that overgrow the dually infected, GFP$^+$ cells arise from preexisting KSHV$^-$ cells. Populations of cells described in Fig. 4 were repeatedly sorted for GFP$^+$ cells (KSHV$^+$/EBV$^+$-fast and KSHV$^+$/EBV$^+$-slow cells, respectively) (gray arrows) and harvested in TRIzol at different time points. RNA was isolated and analyzed with MiXCR to determine the percentage of each clone based on VDJ recombination in the Ig heavy-chain locus. Each clone with a percentage ≥0.5% in the population is represented with a single color. Clones with a percentage <0.5% were combined and their total percentage is represented in gray. The percentage of GFP$^+$ cells at the time of harvest was determined when possible. Samples noted "ND" were directly sorted into TRIzol and the number of GFP$^+$ cells could not be determined.

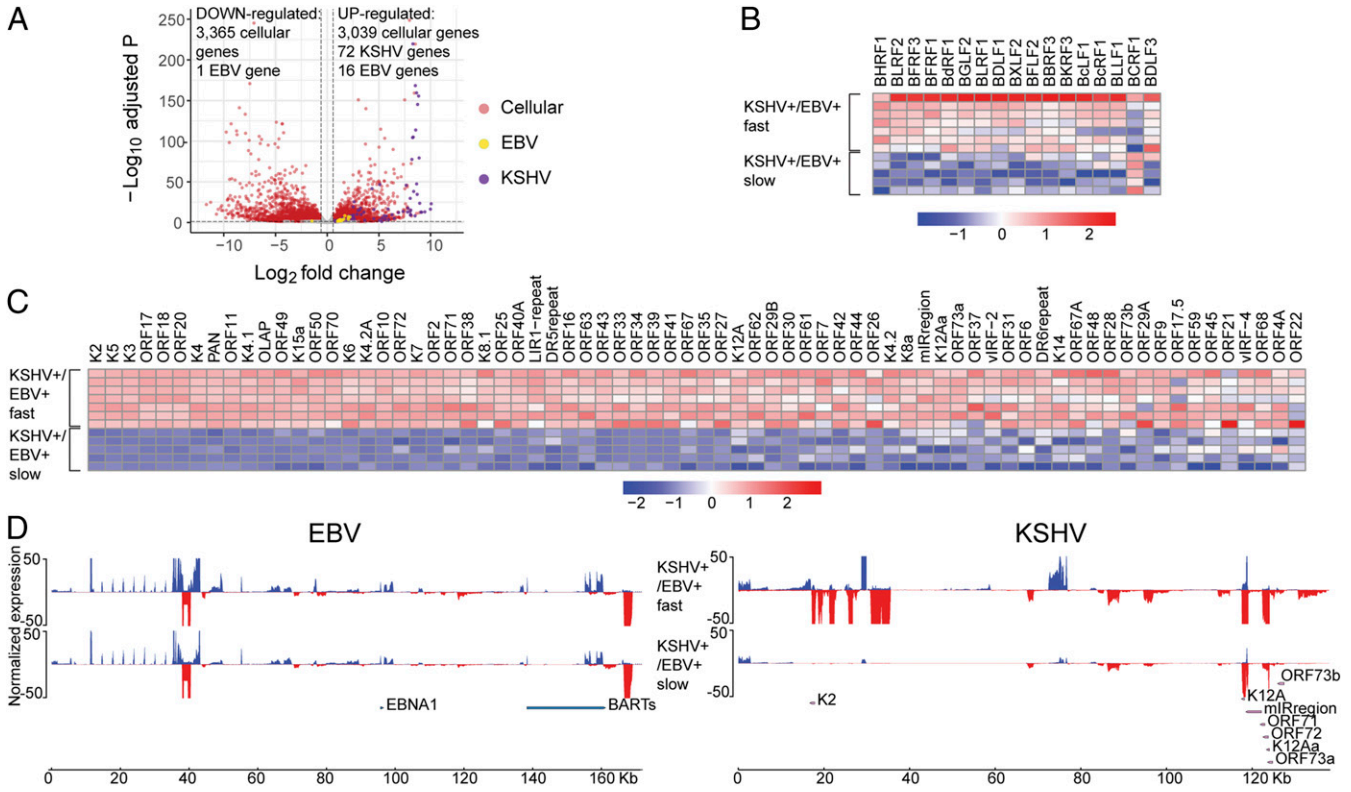

Fig. 6. KSHV gene expression is increased in the KSHV$^+$/EBV$^+$-fast cells. (*A*) Volcano plot of up- and down-regulated cellular and viral genes in dually infected KSHV$^+$/EBV$^+$-fast cells relative to KSHV$^+$/EBV$^+$-slow cells. (*B* and *C*) Heatmaps depicting the normalized expression values of the differentially expressed EBV (*B*) and KSHV (*C*) genes (adjusted $P < 0.05$ and fold-change < -1.5 or >1.5) between the KSHV$^+$/EBV$^+$-fast and KSHV$^+$/EBV$^+$-slow cells for each sample. Genes shown in heatmaps were ordered by *P* value (the gene with the smallest *P* value is on the left of the heatmap). (*D*) Coverage plots of RNA-seq reads of the KSHV$^+$/EBV$^+$-fast and KSHV$^+$/EBV$^+$-slow cells mapped to the forward (blue) or reverse (red) strands of the EBV and KSHV genome. To allow visualization of transcription across the genome, the normalized expression of highly expressed genes was cropped.

cells which contrasted with the similar EBV gene expression in these 2 cell types (Fig. 6*D*).

KSHV$^+$/EBV$^+$-Fast Cells Regulate the Expression of Some Cellular Genes as Do PEL Cells. Principal component analysis (PCA) allows the identification of patterns within complex sets of data. We therefore used PCA to analyze the cellular transcripts in the different types of dually infected, stably transformed cells. Cellular gene expression distinguished the 2 types of dually infected cells (Fig. 7*A*), underscoring the correlation between the differential expression of KSHV genes and cellular genes in these cells. Cellular gene expression in 9 cases of PEL has previously been compared with that in 53 cases of various non-PEL B cell malignancies and a pattern of expression characteristic of PEL has been defined (51). Using gene set enrichment analysis (GSEA), we compared the sets of genes that were up-regulated or down-regulated in PEL and found that cellular genes characteristically inhibited in PEL were also inhibited in the KSHV$^+$/EBV$^+$-fast cells relative to the KSHV$^+$/EBV$^+$-slow cells ($P < 0.001$) (Fig. 7*B*). To determine if differences in the fractions of cells supporting KSHV's lytic phase could underlie these differences in cellular gene expression, the cells supporting KSHV's lytic cycle were measured by counting those with amplified, compartmentalized KSHV DNAs, which are characteristic of its lytic cycle. We used FISH to screen 200 to 300 cells in which 90% or more of the KSHV$^+$/EBV$^+$-fast cells and 30% of the KSHV$^+$/EBV$^+$-slow cells were KSHV$^+$ and found that 1.2% of the KSHV$^+$/EBV$^+$-fast and 0.5% of the KSHV$^+$/EBV$^+$-slow cells displayed amplified KSHV DNA. The increased level of cells in the lytic cycle likely contributes to more lytic mRNAs detected in the KSHV$^+$/EBV$^+$-fast cells while this low overall frequency cannot explain the pronounced inhibition of the subset of cellular RNAs measured in the KSHV$^+$/EBV$^+$-fast cells relative to the KSHV$^+$/EBV$^+$-slow transformed cells. We also measured the fraction of these 2 cell populations supporting EBV's lytic cycle using immunofluorescence and found that 0.6% of the KSHV$^+$/EBV$^+$-fast cells and 0.8% of the KSHV$^+$/EBV$^+$-slow cells expressed the early antigen encoded by BHRF1, indicating that they support entry into EBV's lytic cycle similarly. In addition, measurements with RNA sequencing showed that the levels of the BZLF1 transcript were similar in these 2 cell populations and less than those of EBNA1, already a rare transcript.

Using GSEA, we have also identified cellular genes expressed at higher levels in the KSHV$^+$/EBV$^+$-fast relative to the KSHV$^+$/EBV$^+$-slow cells and found that genes in the pathway involving NF-κB were up-regulated in the KSHV$^+$/EBV$^+$-fast cells ($P < 0.001$) (Fig. 7*C*). Among genes that were up-regulated, we identified CCL20 as well as NFKB1. NF-κB was found to be constitutively activated in PEL cells and its activity was necessary for their survival (52). Increased expression of KSHV genes, in particular v-FLIP, likely contributes to increased NF-κB activity and CCL20 expression in the KSHV$^+$/EBV$^+$-cells (7, 53). This altered expression of viral and cellular genes in the KSHV$^+$/EBV$^+$-fast cells distinguishes their transformed properties from those of the KSHV$^+$/EBV$^+$-slow cells and associates them more closely with PEL cells.

Discussion

PELs are characterized by their being derived from B cells infected with KSHV and in most cases dually infected with EBV. These lymphomas have not been readily modeled in vitro, although multiple studies have detected initial infections, particularly of tonsillar B cells, with KSHV. We set out to determine conditions in which peripheral B cells could be infected with

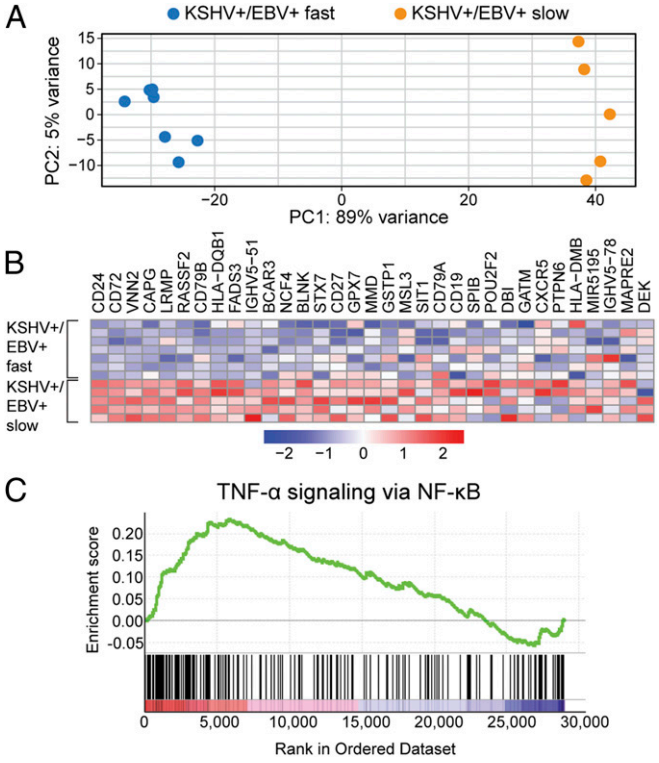

Fig. 7. KSHV$^+$/EBV$^+$-fast cells regulate the expression of some cellular genes as do PEL cells. (*A*) PCA based on cellular transcript reads of 7 samples of KSHV$^+$/EBV$^+$-fast and 5 samples of KSHV$^+$/EBV$^+$-slow cells. (*B*) Heatmap depicting the normalized expression values for the core enriched genes in GSEA analysis of the 7 samples of KSHV$^+$/EBV$^+$-fast cells compared with the 5 samples of KSHV$^+$/EBV$^+$-slow cells from the set of genes down-regulated in PEL (51), $P < 0.001$, false-discovery rate q-value < 0.001. (*C*) GSEA analysis of the 7 samples of KSHV$^+$/EBV$^+$-fast cells compared with the 5 samples of KSHV$^+$/EBV$^+$-slow cells with the hallmark gene set "TNF-α signaling via NF-κB", $P < 0.001$, false-discovery rate q-value < 0.001, normalized enrichment score = 3.8.

KSHV stably both because these cells are readily available and because they are not prone to be activated, as is often the case for portions of tonsillar-derived B cells. We found that an optimal infection of peripheral B cells with KSHV required coinfection by EBV within 24 h. These conditions supported the long-term proliferation of dually infected cells. We found that the infecting EBV partner allowed activation of the B cells and expression of KSHV genes. Analyses with γ-ray irradiation of EBV and with an EBNA2-null variant showed that at least 1 transforming gene of EBV is required for EBV's support of KSHV-infection of B cells. EBV likely also supported proliferation of the dually infected cells given its ability to maintain proliferation of EBV-only infected cells. This likelihood is supported by the findings that forcing the loss of EBV genomes from PEL cells either by inhibiting EBNA1 with its dominant-negative derivative or by targeting EBNA1 with CRISPR/Cas9 gRNAs inhibits both their proliferation and the maintenance of their KSHV genomes (54, 55).

The dually infected cells in populations of B cells varied in their proliferative capacities. Some were outgrown by B cells infected only with EBV and could be isolated by repeated rounds of FACS. These we refer to as KSHV$^+$/EBV$^+$-slow cells. Some dually infected cells outgrew the singly infected cells and are termed KSHV$^+$/EBV$^+$-fast cells. Importantly, both sets of cells maintained both viral genomes indicating that both KSHV and EBV contributed selective advantages to their proliferative and/or survival phenotypes, and thus both were transformed by the dual infection. This understanding underscores the desirability of targeting not only KSHV but also EBV in developing new therapies for PEL.

Both the KSHV$^+$/EBV$^+$-fast cells and the KSHV$^+$/EBV$^+$-slow cells expressed the λ-light chain, which is consistent with the work of Totonchy et al. (27), who showed that KSHV infection induces a B cell receptor revision, resulting in expression of λ-light chain. One study suggested that PELs often have λ–light-chain genes productively rearranged (56). Even though heavy-chain genes are expressed at the RNA level, PELs often do not express surface immunoglobulins detectably (1, 56, 57). We analyzed publicly available data from RNA sequencing of PEL cell lines with MiXCR and confirmed the previously reported use of λ-light chain in BCBL-1 cells and κ-light chain in HBL-6 cells (56). In addition, we found BC-3 and AP3 cells to express λ-light chain, too. The Ig light chain used in other analyzed PEL cell lines (AP5 and AP2) could not be determined due to its low or absent expression. Thus, 3 of 4 PEL cell lines express λ–light-chain mRNA as do both the KSHV$^+$/EBV$^+$-fast and the KSHV$^+$/EBV$^+$-slow transformed cells.

The analysis of RNAs expressed in multiple samples of the KSHV$^+$/EBV$^+$-fast and the KSHV$^+$/EBV$^+$-slow cells revealed that the KSHV$^+$/EBV$^+$-fast cells have distinct, transformed properties. It showed that the KSHV$^+$/EBV$^+$-fast cells express higher levels of KSHV viral latent and lytic genes. KSHV latency locus and viral IL-6 genes, which are expressed in PEL, were among those genes up-regulated in the KSHV$^+$/EBV$^+$-fast cells. Furthermore, GSEA analysis showed that cellular genes characteristically inhibited in PEL were also inhibited in the KSHV$^+$/EBV$^+$-fast cells relative to the KSHV$^+$/EBV$^+$-slow cells. In addition, NF-κB activity, which is essential for the survival of PEL cells (52), was increased in the KSHV$^+$/EBV$^+$-fast cells. These 3 characteristics define KSHV$^+$/EBV$^+$-fast cells' distinct, transformed properties, associating them with features of bona fide PEL cells.

The characteristic transformation of the KSHV$^+$/EBV$^+$-fast cells likely results from their increased expression of the KSHV transforming genes. KSHV vIL-6 acts in an autocrine loop and PEL cells depend on this viral cytokine for proliferation and survival (49, 50). Increased expression of KSHV vIL-6 could therefore drive the transformation of the KSHV$^+$/EBV$^+$-fast cells. In addition, increased expression of KSHV v-FLIP likely contributes to the increased NF-κB activity and to the transformed phenotype of these cells (7, 53). Another insight into this transformation comes from the finding that it is not necessary for KSHV to express its lytic genes to infect B cells optimally along with EBV. This subset of viral genes therefore is not needed for the early events in transformation.

The long-term dual infection and transformation of peripheral B cells by KSHV and EBV advances our ability to identify steps in a progression toward PEL. For example, neither the KSHV$^+$/EBV$^+$-fast nor the KSHV$^+$/EBV$^+$-slow cells support either viral lytic phase efficiently. We can now identify the viral genes that regulate the expression of cellular genes in patterns shared with PEL. In a recent study, NSG mice that were reconstituted with human CD34$^+$ cells and subsequently infected with KSHV and EBV showed enhanced tumor formation compared with mice infected with EBV only (30). By selecting for tumors in immunodeficient mice, McHugh et al. (30) observed a correlation between the fraction of cells that supported EBV's lytic cycle and tumor formation. It is particularly revealing that the distinct, transformed properties of the KSHV$^+$/EBV$^+$-fast cells arose in the absence of any selective pressures in an animal or human host and did not correlate with a dramatic increase in the fraction of cells supporting EBV's lytic cycle. Our model of dual infection in vitro therefore enables the genetic dissection of the viral and cellular genes that mediate the early stages of transformation toward PEL.

Materials and Methods

Isolation of Peripheral B Cells. Peripheral blood B lymphocytes were purified from whole blood collected from healthy donors and buffy coats obtained from Interstate Blood Bank. Study protocols were approved by the University of Wisconsin–Madison Health Sciences Minimal Risk Institutional Review Board. Informed consent was obtained from all donors. PBMCs were isolated from EDTA-treated blood by Ficoll-Paque (GE Healthcare Life Sciences) density gradient separation. Twelve different donors were used in this study and each condition for which $n \geq 3$ was tested in 3 to 4 different donors. Peripheral

$CD19^+$ B cells were purified from PBMCs by negative selection according to the instructions of the manufacturer (B Cell Isolation Kit II, Human, Miltenyi Biotec). The isolation yielded > 90% $CD19^+$ B cells as determined by staining with anti-CD19 monoclonal antibody and flow cytometry.

Cell Culture. The 293 (58) and Daudi (59) cell lines were used for titration of KSHV and the recombinant 2089 strain of EBV, respectively. LL8 CD40 ligand feeder cells (60, 61) were used for in vitro activation of peripheral B cells. 293 cells and LL8 CD40 ligand feeder cells were grown in DMEM supplemented with 10% FBS. Daudi cells and peripheral B cells were cultured in RPMI supplemented with 10% FBS. Antibiotics (200 U/mL penicillin and 200 μg/mL streptomycin) were added to all cell lines and primary cultures. All cells were incubated in 5% CO_2 at 37 °C. All cells used in this study were routinely tested for mycoplasma contamination using the primers described by van Kuppeveld et al. (62).

Antibodies. Anti-CD19 antibody clone LT19 conjugated to APC or VioBlue was purchased from Miltenyi Biotec. Two anti–DC-SIGN antibodies and their respective isotype controls were used: anti-human DC-SIGN/CD209 clone 120507 and mouse IgG2B isotype control conjugated to APC (R&D Systems) and anti-human DC-SIGN/CD209 clone DCN46 and mouse IgG2b, κ-isotype control conjugated to V450 (BD Biosciences). The anti-EBV EA-R-p17 antibody, clone 5B11 from Millipore Sigma was used to detect expression of the early antigen encoded by BHRF1. The anti-gpK8.1A 4A4 antibody (hybridoma culture supernatant) was a kind gift from Bala Chandran, Department of Molecular Medicine, Morsani College of Medicine, University of South Florida, Tampa, FL.

KSHV and EBV Virus Stocks Preparation. iSLK cells (18) carrying the recombinant wild-type KSHV BAC16 (31) or the mutant KSHV BAC16RTAStop (45) (iSLKBAC16 and iSLKBAC16RTAstop cells were kindly provided by Jae U. Jung, Department of Molecular Microbiology and Immunology, Keck School of Medicine, University of Southern California, Los Angeles, CA) were grown in DMEM supplemented with 10% FBS, 250 μg/mL G418, 1 μg/mL puromycin, and 1,200 μg/mL hygromycin. One clone of iSLKBAC16 cells (clone 5) was isolated and used in this study to produce KSHV BAC16 virus. iSLKBAC16 clone 5 and iSLKBAC16RTAstop cells were induced with 1 μg/mL doxycycline and 1 mM valproic acid in the absence of G418, puromycin, and hygromycin. The supernatant was harvested at days 4 and 8 and cleared of cells and debris by multiple rounds of centrifugation (500 × *g* for 10 min followed by 3,000 × *g* for 10 min). B95-8 (63) and HH514 clone 16 cells were grown in RPMI supplemented with 10% FBS and were induced when they reached 7×10^5 cells/mL with 20 ng/mL TPA and 3.5 mM sodium butyrate. The supernatant was collected at day 5 and cells and debris were removed by centrifugation at 500 × *g* for 10 min and filtration with a 0.8-μm low-protein binding filter. The 293 cells carrying the recombinant EBV genome 2089 (64) were grown in DMEM supplemented with 10% FBS. To induce viral production, cells were transfected when they were ∼50 to 60% confluent with vectors expressing BZLF1 and BARF4 using Lipofectamine 2000 (Invitrogen). Following transfection, the medium was changed to DMEM with 10% FBS and the supernatant was harvested 5 d later. Alternatively, 293 cells carrying 2089 and expressing BZLF1 fused to the estrogen receptor ligand-binding domain were cultured in DMEM supplemented with 10% FBS, 1 μg/mL puromycin, and 200 μg/mL hygromycin. Virus production was induced with 200 nM tamoxifen, the medium was removed 24 h later and changed to DMEM with 10% FBS. The supernatant was collected 2 and 4 d later. Supernatants containing 2089 virus were cleared of cells and debris by multiple rounds of centrifugation (500 × *g* for 10 min followed by 3,000 × *g* for 10 min). All viruses were maintained at a pH of 7.2 by addition of Hepes when necessary. KSHV and EBV viral supernatants were concentrated 100-fold by centrifugation at 48,000 × *g* for 2 h and viral pellets were resuspended at 4 °C overnight in RPMI supplemented with 10% FBS and 50 mM Hepes. Separate aliquots were kept at −80 °C and thawed immediately before use; another round of centrifugation at 950 × *g* for 10 min was performed before use for KSHV and 2089 viral preparations to remove any remaining debris.

Titration of Virus Stocks by Real-Time PCR and Infectivity Assays. The number of KSHV and EBV physical particles in viral stocks was measured by real-time PCR. Viral stocks were treated with DNase I (Roche) and proteinase K (Roche) before viral DNA extraction by Phenol/Chloroform. An aliquot of 4 μL of isolated viral DNA was analyzed by real-time PCR as previously described (5). Briefly, reactions were performed in a 384-well plate in a final volume of 20 μL with 0.5 μM of both the forward and reverse primer, 0.2 μM of the probe, Rox reference dye (Invitrogen), and AmpliTaq Gold 360 Master Mix (Applied Biosystems). Primers and probes for real-time PCR were as follows: BALF5 (EBV), forward: 5′-CGG AAG CCC TCT GGA CTT C-3′, reverse: 5′-CCC TGT TTA TCC GAT GGA ATG-3′, probe: 5′-6-FAM/TGT ACA CGC ACG AGA AAT GCG CC/TAMRA-3′; LANA1 (KSHV), forward: 5′-AAC AAA TTG CCA GTA GCC CAC CAG-3′, reverse: 5′-TAA CTG GAA CGC GCC TCA TAC GAA-3′, probe: 5′-6-FAM/ATA CAC CAG/ZEN/ACG ATG ACC CAC AAC CT/IABkFQ-3′. The reactions were incubated at 50 °C for 2 min, then at 95 °C for 10 min followed by 40 cycles of 95 °C for 15 s and 60 °C for 1 min. Data were collected on a 7900HT real-time instrument (Applied Biosystems) and analyzed using SDS v2.4 software. The number of viral particles was determined by creating a standard curve using linearized plasmids containing the DNA sequence of either BALF5 or LANA1.

For KSHV and 2089 viral stocks, the number of infectious particles was determined on 293 and Daudi cells, respectively. Briefly, 293 or Daudi cells were incubated with serially diluted virus for 1 h at 4 °C. Following incubation, additional medium (DMEM or RPMI with 10% FBS and 50 mM Hepes) was added and cells and virus were incubated for an additional 72 h at 37 °C. The number of GFP^+ cells was determined by fluorescence microscopy. The number of infectious viral particles was calculated by multiplying the percentage of GFP^+ cells by the total number of cells at the time of infection. For B95-8 viral stocks, an MOI of 1 was determined by the amount of virus needed for ∼60% of peripheral B cells to become blasts in 72 h and for HH514 clone 16 viral stocks, by the amount of virus needed for ∼60% of peripheral B cells to express the early antigen encoded by BHRF1 scored by immunofluorescence. For all viral stocks used in this study, approximately 1 in 100 to 1 in 200 physical particles was infectious.

γ-Irradiation of Virus Stocks. Stocks of B95-8 virus were irradiated with γ-rays from a ^{137}Cs source for increasing times at a fixed position in the presence of 1 mM histidine, which served as a free-radical scavenger. The exposure times were determined by the flux of γ-rays previously measured at that position and corrected for the decay of ^{137}Cs since that measurement.

PCR to Identify Wild-Type and Mutant KSHV BAC16 Strains. DNA was isolated from mutant and wild-type KSHV BAC16 viral particles as described above. A fragment of 476 bp spanning the mutation in ORF50 was amplified by PCR with the GoTaq Flexi DNA Polymerase (Promega) at the following conditions: denaturation at 95 °C for 1 min, annealing at 60 °C for 1 min, and extension at 72 °C for 1 min for 35 cycles using the forward primer: 5′-ACG TGG CAG TCT GGA TTG AG-3′ and the reverse primer: 5′-AAT GCC TTG GGA TGC CTC TG-3′. The PCR product was purified using the QIAquick PCR Purification Kit (Qiagen) and digested with the NheI restriction enzyme for 2 h at 37 °C.

Infection and In Vitro Activation of Peripheral B Cells. In each experiment, 1.5×10^5–2×10^6 B cells were used per condition. In all experiments, a fraction of the cells was left uninfected as a negative control and no cell growth or GFP expression was observed. During incubation with viruses, 50 mM Hepes was added to the culture medium of peripheral B cells. For exposure to KSHV, the recombinant wild-type or mutant KSHV BAC16 virus was added to B cells at an MOI of 2 to 3 and cells and virus were centrifugated at 950 × *g* for 90 min at room temperature (65). Following spinoculation, cells were washed to remove unbound viruses and resuspended in their culture medium. For experiments in which a neutralizing antibody was used, B cells were exposed to KSHV BAC16 at an MOI of 2 as described above. Cells were washed to remove excess, unbound virus and treated 24 h later with anti-gpK8.1A 4A4 for 2 h at 37 °C. Cells were then washed and infected with EBV. For exposure to EBV, B cells were exposed to B95-8 or HH514 clone 16 virus at an MOI of 1 to 2 or 2089 at an MOI of 3 for 1 h at 4 °C, washed and resuspended in their culture medium. Infection with 2089 virus was only used as a positive control for flow cytometry. For experiments of in vitro activation of B cells, B cells were plated on top of irradiated or mitomycin C-treated LL8 CD40 ligand feeder cells and grown in RPMI supplemented with 10% FBS, 100 nM sodium selenite and 2 ng/mL IL-4 (R&D Systems, Recombinant Human IL-4).

Flow Cytometry. Peripheral B cells were stained with the Ghost Dye Red 780 viability dye and anti-CD19 monoclonal antibody conjugated to APC according to the manufacturers' protocols (TONBO Biosciences and Miltenyi Biotec, respectively). For measuring DC-SIGN expression, cells were stained with the Ghost Dye Red 780 viability dye, anti-CD19 monoclonal antibody conjugated to APC or VioBlue and anti-DC-SIGN monoclonal antibody clone DCN46 conjugated to V450 or clone 120507 conjugated to APC and their respective isotype controls. For all staining procedures, the buffer used contained 1× PBS pH 7.2, 0.5% BSA and 2 mM EDTA. While staining with antibodies, 100 μg/mL mouse IgG (Jackson ImmunoResearch) was added to block nonspecific binding. Appropriate compensation and fluorescence-minus-one controls were used. Infection with KSHV was determined by GFP expression. For gating of GFP^+ cells, peripheral B cells were infected with the B95-8 strain of EBV as a negative control and the recombinant 2089 strain of EBV as a positive control. At least 10,000 cells were analyzed

per condition on a BD LSR Fortessa cytometer and data analysis was performed using FLowJo software. For sorting of GFP$^+$ cells, cells were sorted on a BD FACSAria II BSL-2 cell sorter.

Quantification of the Number of GFP$^+$ Cells in Populations of Infected B Cells by Fluorescence Microscopy. The number of GFP$^+$ cells was counted at different time points using fluorescence microscopy. Peripheral B cells were stained with Trypan blue and the number of live cells was measured with a hematocytometer at the same time points. Cells were passaged as needed and the dilution factor was monitored to calculate the number of doublings.

Quantification of the Number of EBV and KSHV Genomes per Cell in Infected B Cells by Real-Time PCR. Infected peripheral B cells were harvested in TRIzol or TRIzol LS (Invitrogen). DNA was isolated from lysed cells following the protocol from Invitrogen. For each sample, ∼100 ng of purified total DNA was analyzed by real-time PCR as described above. The number of viral DNA copies per cell was estimated by measuring the number of molecules of EBV, KSHV, and rhodopsin in each sample. Standard curves were created using linearized plasmids containing the DNA sequence of either BALF5, LANA1, or rhodopsin. The primers used for detection of EBV and KSHV DNA are listed above. Primers and probes for rhodopsin were as follows: forward: 5′-ATC AGG AAC CAT TGC CAC GTC CTA-3′, reverse: 5′-AGG CCA AAG ATG GAC ACA CAG AGT-3′, probe: 5′-6-FAM/AGC CTC TAG/ZEN/TTT CCA GAA GCT GCA CA/IABkFQ-3′.

FISH. Cells were fixed and hybridized with probes as previously described (6, 66). In brief, cells were treated with 0.075 M KCl for 20 min at 37 °C, fixed in methanol:acetic acid at a 3:1 ratio for 30 min at room temperature, and spread on cold slides. Slides were dried and prehybridized in a buffer with 2× SSC and 0.5% (vol/vol) Nonidet P-40 (Sigma-Aldrich) for 30 min at 37 °C, dehydrated in a cold ethanol series (70%, 80%, and 95%) for 2 min each, air-dried at 50 °C, denatured in a buffer with 70% formamide and 2× SSC, pH 5.3, for 2 min at 72 °C followed by dehydration with a cold ethanol series, and air-dried. The KSHV cosmid Z8 (67) was labeled with biotin-16-dUTP (Roche), and EBV p135.16 was labeled with digoxigenin-11-2′-deoxy-uridine-5′-triphosphate (Roche) by nick translation as hybridization probes for detection of KSHV and EBV genomes in cells, respectively. Next, 200 ng of the labeled probe was precipitated along with 6 μg Salmon Sperm DNA (Invitrogen) and 4 μg Human Cot-1 DNA (Invitrogen) and resuspended in CEP hybridization buffer (55% formamide, 1× SSC, pH 7.0, and 10% dextran sulfate) followed by denaturation at 70 °C for 10 min. Forty-five nanograms of the probe was then hybridized with each sample at 37 °C overnight in a moist chamber. The slides were washed twice in 2× SSC containing 50% formamide for 30 min at 50 °C and twice in 2× SSC for 30 min at 50 °C. The hybridized probe was detected by incubation with 10 μL of a detection solution containing a mouse monoclonal antidigoxin–FITC conjugate (Sigma-Aldrich) and a streptavidin-Cy3 conjugate (Sigma-Aldrich) for 20 min at 37 °C. The slides were washed twice in 4× SSC containing 0.05% Triton X-100 for 5 min at room temperature and mounted in Vectashield mounting medium with DAPI (Vector Laboratories) for staining chromosomes. The percentage of KSHV$^+$ and EBV$^+$ cells as well as the number of plasmids per cell were determined by counting the number of signals in at least 45 cells for each sample. FISH slides were imaged on an Axiovert 200M microscope and AxioVision software (Zeiss) was used for acquisition of the images. Images were digitally processed for presentation with Adobe Photoshop.

Immunofluorescence. Cells were pelleted and resuspended in 1× PBS before being air-dried on slides. Cells were then fixed in ice-cold acetone and incubated overnight in blocking solution (PBS + 10% goat serum). Cells were then incubated with the primary antibody diluted 1:100 in PBS + 10% goat serum for 1 h at 37 °C. Cells were washed with PBS and incubated with the secondary antibody (Alexa Fluor 568 F(ab')2 goat anti-mouse IgG (H+L), ThermoFisher) diluted 1:2,000 in PBS + 10% goat serum for 1 h at 37 °C. Cells were washed with PBS and the slides were mounted in Vectashield mounting medium with DAPI (Vector Laboratories).

RNA Isolation for RNA-Sequencing. Dually infected B cells were harvested in TRIzol or TRIzol LS (Invitrogen). RNA was isolated using the Direct-zol RNA MiniPrep Kit (Zymo Research) and RNA quality was assessed using an Agilent 2100 Bioanalyzer.

Library Preparation and High-Throughput Sequencing. Library preparation and sequencing on an Illumina NovaSeq. 6000 with paired-end 150-bp reads was performed by the Oklahoma Medical Research Foundation Clinical Genomics Center (Oklahoma City, OK). Raw data and additional methods were deposited in the Sequence Read Archive (PRJNA544266).

RNA-Seq Analysis. Reads were mapped to the NCI Genomic Data Commons (GDC) reference genome with STAR_2.5.1b (68). Parameters for first and second pass mapping were selected from the GDC Harmonized mRNA Analysis Pipeline. Reads mapping to cellular and viral genes were quantified with featureCounts v1.6.2 (69). For cellular genes, the GENCODE v22 GTF annotation was used. Viral gene counts were determined using a modification of the approach by Bruce et al. (47). Briefly, reads mapping to the unique coding sequence (UCDS) region of each KSHV gene were summed [UCDS regions were obtained from Bruce et al. (47)]. For nested transcripts, an estimated count of the overlapping portion of the larger transcript B was subtracted from the raw count of the UCDS region of the smaller transcript A using the formula: $\text{Counts}(\text{UCDS}_A) = \text{RawCounts}(\text{UCDS}_A) - [\text{RawCounts}(\text{UCDS}_B) \times (\text{Length}(\text{UCDS}_A)/\text{Length}(\text{UCDS}_B))]$. A similar approach was applied to EBV. UCDS regions were demarcated using the National Center for Biotechnology Information reference NC_007605.1 and regions identified by Eric Johannsen (*SI Appendix*, Table S3). Where possible, nonoverlapping regions were identified and separated by at least 152 bp. When transcript structure prohibited this approach, nested transcripts were identified and quantified as described above. Following this approach, only 0.7–3.1% of viral reads were unassigned to a specific transcript by featureCounts. For differential expression analysis, data normalization, model fitting, and fold-change calculations were performed in R (3.5.1) with DESeq2 v1.22.1 (70). Genes with fewer than 10 reads across all samples were omitted from the analysis. Fold-change shrinkage was applied using the apeglm method (71). In heatmaps, the coloring is the columnwise *z*-scores of the variance-stabilizing transformation. The normalized expression in the coverage plots of RNA-seq reads was plotted using deepTools factoring in the total number of mapped reads (in millions) for each group of samples (7 samples of KSHV$^+$/EBV$^+$-fast cells and 5 samples of KSHV$^+$/EBV$^+$-slow cells). GSEA was performed with GSEA v3.0 (72, 73) with gene sets obtained from Klein et al. (51) (genes down-regulated or up-regulated in PEL) and MSigDB hallmark gene sets (database v6.2) (74). Gene expression from the DESeq2 comparison of the KSHV$^+$/EBV$^+$-fast cells vs. the KSHV$^+$/EBV$^+$-slow cells was ranked with ranking metric −log(*P* value)*sign(log fold-change) using GSEA PreRanked. Ig clonotypes were determined using MiXCR v2.1.11 (75) with built-in V/D/J/C library: repseqio.v1.5. The recommended pipeline for RNA-seq input was used. Clonotypes were determined using the IGH VDJ (CDR3) calls from MiXCR. The percentage of each Ig heavy and light chain in the different populations of cells was obtained from the MiXCR IGH and IGK/IGL results, respectively. Publicly available datasets for KSHV$^+$ primary effusion lymphomas were obtained from the Sequence Read Archive (PRJEB18662, PRJNA352335, PRJNA362820).

Statistics. The program Mstat, v6.3 or v6.4, was used for statistical analyses (N. Drinkwater, McArdle Laboratory for Cancer Research, School of Medicine and Public Health, University of Wisconsin) and is available for download (https://mcardle.wisc.edu/mstat/). For analysis of flow cytometry data, at least 3 biological replicates were used for statistical analyses.

ACKNOWLEDGMENTS. We thank Dr. Jae U. Jung and Dr. Bala Chandran for providing reagents; Manjistha Ahooja for her help in the production of virus stocks; Dr. Ya-Fang Chiu, Dr. Ngan Lam, and Dr. Asuka Nanbo for help with obtaining blood, experimental insights, and suggestions; Dr. Eric Johannsen for the use of computer hardware and Epstein–Barr virus annotations; Dr. Julien Henry for help with programming tasks; and Drs. Paul Ahlquist, Eric Johannsen, Nate Sherer, Ya-Fang Chiu, Bill Dove, and our laboratory colleagues for careful review of the manuscript. This work was supported by the NIH Grant P01 CA022443. Flow cytometry experiments were performed thanks to the University of Wisconsin Carbone Cancer Center Support Grant P30 CA014520 and NIH Grant 1S100OD018202-01. The authors declare no competing financial interests. B.S. is an American Cancer Society Research Professor.

1. R. G. Nador *et al*., Primary effusion lymphoma: A distinct clinicopathologic entity associated with the Kaposi's sarcoma-associated herpes virus. *Blood* **88**, 645–656 (1996).
2. Y.-B. Chen, A. Rahemtullah, E. Hochberg, Primary effusion lymphoma. *Oncologist* **12**, 569–576 (2007).
3. E. Cesarman, D. M. Knowles, The role of Kaposi's sarcoma-associated herpesvirus (KSHV/HHV-8) in lymphoproliferative diseases. *Semin. Cancer Biol.* **9**, 165–174 (1999).
4. D. Vereide, B. Sugden, Insights into the evolution of lymphomas induced by Epstein-Barr virus. *Adv. Cancer Res.* **108**, 1–19 (2010).
5. D. T. Vereide, B. Sugden, Lymphomas differ in their dependence on Epstein-Barr virus. *Blood* **117**, 1977–1985 (2011).
6. Y. F. Chiu, A. U. Sugden, K. Fox, M. Hayes, B. Sugden, Kaposi's sarcoma-associated herpesvirus stably clusters its genomes across generations to maintain itself extrachromosomally. *J. Cell Biol.* **216**, 2745–2758 (2017).

7. I. Guasparri, S. A. Keller, E. Cesarman, KSHV vFLIP is essential for the survival of infected lymphoma cells. *J. Exp. Med.* **199**, 993–1003 (2004).
8. E. Wies *et al*., The viral interferon-regulatory factor-3 is required for the survival of KSHV-infected primary effusion lymphoma cells. *Blood* **111**, 320–327 (2008).
9. A. Godfrey, J. Anderson, A. Papanastasiou, Y. Takeuchi, C. Boshoff, Inhibiting primary effusion lymphoma by lentiviral vectors encoding short hairpin RNA. *Blood* **105**, 2510–2518 (2005).
10. Y. Chang *et al*., Identification of herpesvirus-like DNA sequences in AIDS-associated Kaposi's sarcoma. *Science* **266**, 1865–1869 (1994).
11. N. Dupin *et al*., Herpesvirus-like DNA sequences in patients with Mediterranean Kaposi's sarcoma. *Lancet* **345**, 761–762 (1995).
12. P. S. Moore, Y. Chang, Detection of herpesvirus-like DNA sequences in Kaposi's sarcoma in patients with and those without HIV infection. *N. Engl. J. Med.* **332**, 1181–1185 (1995).
13. C. Boshoff *et al*., Kaposi's sarcoma-associated herpesvirus infects endothelial and spindle cells. *Nat. Med.* **1**, 1274–1278 (1995).
14. J. A. Ambroziak *et al*., Herpes-like sequences in HIV-infected and uninfected Kaposi's sarcoma patients. *Science* **268**, 582–583 (1995).
15. D. J. Blackbourn *et al*., Infectious human herpesvirus 8 in a healthy North American blood donor. *Lancet* **349**, 609–611 (1997).
16. L. L. Decker *et al*., The Kaposi sarcoma-associated herpesvirus (KSHV) is present as an intact latent genome in KS tissue but replicates in the peripheral blood mononuclear cells of KS patients. *J. Exp. Med.* **184**, 283–288 (1996).
17. J. Soulier *et al*., Kaposi's sarcoma-associated herpesvirus-like DNA sequences in multicentric Castleman's disease. *Blood* **86**, 1276–1280 (1995).
18. J. Myoung, D. Ganem, Generation of a doxycycline-inducible KSHV producer cell line of endothelial origin: Maintenance of tight latency with efficient reactivation upon induction. *J. Virol. Methods* **174**, 12–21 (2011).
19. R. Renne, D. Blackbourn, D. Whitby, J. Levy, D. Ganem, Limited transmission of Kaposi's sarcoma-associated herpesvirus in cultured cells. *J. Virol.* **72**, 5182–5188 (1998).
20. J. T. Bechtel, Y. Liang, J. Hvidding, D. Ganem, Host range of Kaposi's sarcoma-associated herpesvirus in cultured cells. *J. Virol.* **77**, 6474–6481 (2003).
21. D. J. Blackbourn *et al*., The restricted cellular host range of human herpesvirus 8. *AIDS* **14**, 1123–1133 (2000).
22. E. A. Mesri *et al*., Human herpesvirus-8/Kaposi's sarcoma-associated herpesvirus is a new transmissible virus that infects B cells. *J. Exp. Med.* **183**, 2385–2390 (1996).
23. S. M. Nicol *et al*., Primary B lymphocytes infected with Kaposi's sarcoma-associated herpesvirus can be expanded in vitro and are recognized by LANA-specific CD4+ T cells. *J. Virol.* **90**, 3849–3859 (2016).
24. L. M. Hassman, T. J. Ellison, D. H. Kedes, KSHV infects a subset of human tonsillar B cells, driving proliferation and plasmablast differentiation. *J. Clin. Invest.* **121**, 752–768 (2011).
25. J. Myoung, D. Ganem, Active lytic infection of human primary tonsillar B cells by KSHV and its noncytolytic control by activated CD4+ T cells. *J. Clin. Invest.* **121**, 1130–1140 (2011).
26. J. Myoung, D. Ganem, Infection of primary human tonsillar lymphoid cells by KSHV reveals frequent but abortive infection of T cells. *Virology* **413**, 1–11 (2011).
27. J. Totonchy *et al*., KSHV induces immunoglobulin rearrangements in mature B lymphocytes. *PLoS Pathog.* **14**, e1006967 (2018).
28. D. J. Moss, J. H. Pope, Assay of the infectivity of Epstein-Barr virus by transformation of human leucocytes in vitro. *J. Gen. Virol.* **17**, 233–236 (1972).
29. B. Sugden, W. Mark, Clonal transformation of adult human leukocytes by Epstein-Barr virus. *J. Virol.* **23**, 503–508 (1977).
30. D. McHugh *et al*., Persistent KSHV infection increases EBV-associated tumor formation in vivo via enhanced EBV lytic gene expression. *Cell Host Microbe* **22**, 61–73.e7 (2017).
31. K. F. Brulois *et al*., Construction and manipulation of a new Kaposi's sarcoma-associated herpesvirus bacterial artificial chromosome clone. *J. Virol.* **86**, 9708–9720 (2012).
32. G. Rappocciolo *et al*., Human herpesvirus 8 infects and replicates in primary cultures of activated B lymphocytes through DC-SIGN. *J. Virol.* **82**, 4793–4806 (2008).
33. S. Chakraborty, M. V. Veettil, B. Chandran, Kaposi's sarcoma associated herpesvirus entry into target cells. *Front. Microbiol.* **3**, 6 (2012).
34. M. V. Veettil, C. Bandyopadhyay, D. Dutta, B. Chandran, Interaction of KSHV with host cell surface receptors and cell entry. *Viruses* **6**, 4024–4046 (2014).
35. C. Jin *et al*., Multiple signaling pathways are involved in the interleukine-4 regulated expression of DC-SIGN in THP-1 cell line. *J. Biomed. Biotechnol.* **2012**, 357060 (2012).
36. T. Kadowaki, H. Inagawa, C. Kohchi, M. Hirashima, G. Soma, Functional characterization of lipopolysaccharide derived from symbiotic bacteria in rice as a macrophage-activating substance. *Anticancer Res.* **31**, 2467–2476 (2011).
37. F.-Z. Wang, S. M. Akula, N. P. Pramod, L. Zeng, B. Chandran, Human herpesvirus 8 envelope glycoprotein K8.1A interaction with the target cells involves heparan sulfate. *J. Virol.* **75**, 7517–7527 (2001).
38. A. Birkmann *et al*., Cell surface heparan sulfate is a receptor for human herpesvirus 8 and interacts with envelope glycoprotein K8.1. *J. Virol.* **75**, 11583–11593 (2001).
39. R. E. Luna *et al*., Kaposi's sarcoma-associated herpesvirus glycoprotein K8.1 is dispensable for virus entry. *J. Virol.* **78**, 6389–6398 (2004).
40. R. F. Kalejta, Functions of human cytomegalovirus tegument proteins prior to immediate early gene expression. *Curr. Top. Microbiol. Immunol.* **325**, 101–115 (2008).
41. S. Jochum, R. Ruiss, A. Moosmann, W. Hammerschmidt, R. Zeidler, RNAs in Epstein-Barr virions control early steps of infection. *Proc. Natl. Acad. Sci. U.S.A.* **109**, E1396–E1404 (2012).
42. W. Mark, B. Sugden, Transformation of lymphocytes by Epstein-Barr virus requires only one-fourth of the viral genome. *Virology* **122**, 431–443 (1982).
43. M. Rabson, L. Heston, G. Miller, Identification of a rare Epstein-Barr virus variant that enhances early antigen expression in Raji cells. *Proc. Natl. Acad. Sci. U.S.A.* **80**, 2762–2766 (1983).
44. W. Hammerschmidt, B. Sugden, Genetic analysis of immortalizing functions of Epstein-Barr virus in human B lymphocytes. *Nature* **340**, 393–397 (1989).
45. Z. Toth *et al*., Negative elongation factor-mediated suppression of RNA polymerase II elongation of Kaposi's sarcoma-associated herpesvirus lytic gene expression. *J. Virol.* **86**, 9696–9707 (2012).
46. A. Faure *et al*., How Kaposi's sarcoma-associated herpesvirus stably transforms peripheral B cells towards Lymphomagenesis. NCBI SRA. https://www.ncbi.nlm.nih.gov/sra/PRJNA544266. Deposited 22 May 2019.
47. A. G. Bruce *et al*., Quantitative analysis of the KSHV transcriptome following primary infection of blood and lymphatic endothelial cells. *Pathogens* **6**, E11 (2017).
48. D. Dittmer *et al*., A cluster of latently expressed genes in Kaposi's sarcoma-associated herpesvirus. *J. Virol.* **72**, 8309–8315 (1998).
49. M. Chatterjee, J. Osborne, G. Bestetti, Y. Chang, P. S. Moore, Viral IL-6-induced cell proliferation and immune evasion of interferon activity. *Science* **298**, 1432–1435 (2002).
50. K. D. Jones *et al*., Involvement of interleukin-10 (IL-10) and viral IL-6 in the spontaneous growth of Kaposi's sarcoma herpesvirus-associated infected primary effusion lymphoma cells. *Blood* **94**, 2871–2879 (1999).
51. U. Klein *et al*., Gene expression profile analysis of AIDS-related primary effusion lymphoma (PEL) suggests a plasmablastic derivation and identifies PEL-specific transcripts. *Blood* **101**, 4115–4121 (2003).
52. S. A. Keller, E. J. Schattner, E. Cesarman, Inhibition of NF-kappaB induces apoptosis of KSHV-infected primary effusion lymphoma cells. *Blood* **96**, 2537–2542 (2000).
53. V. Punj *et al*., Induction of CCL20 production by Kaposi sarcoma-associated herpesvirus: Role of viral FLICE inhibitory protein K13-induced NF-kappaB activation. *Blood* **113**, 5660–5668 (2009).
54. A. A. Mack, B. Sugden, EBV is necessary for proliferation of dually infected primary effusion lymphoma cells. *Cancer Res.* **68**, 6963–6968 (2008).
55. R. Bigi *et al*., Epstein-Barr virus enhances genome maintenance of Kaposi sarcoma-associated herpesvirus. *Proc. Natl. Acad. Sci. U.S.A.* **115**, E11379–E11387 (2018).
56. F. Fais *et al*., Immunoglobulin V region gene use and structure suggest antigen selection in AIDS-related primary effusion lymphomas. *Leukemia* **13**, 1093–1099 (1999).
57. A. Matolcsy, R. G. Nádor, E. Cesarman, D. M. Knowles, Immunoglobulin VH gene mutational analysis suggests that primary effusion lymphomas derive from different stages of B cell maturation. *Am. J. Pathol.* **153**, 1609–1614 (1998).
58. F. L. Graham, J. Smiley, W. C. Russell, R. Nairn, Characteristics of a human cell line transformed by DNA from human adenovirus type 5. *J. Gen. Virol.* **36**, 59–74 (1977).
59. A. Nanbo, K. Inoue, K. Adachi-Takasawa, K. Takada, Epstein-Barr virus RNA confers resistance to interferon-α-induced apoptosis in Burkitt's lymphoma. *EMBO J.* **21**, 954–965 (2002).
60. P. Garrone *et al*., Fas ligation induces apoptosis of CD40-activated human B lymphocytes. *J. Exp. Med.* **182**, 1265–1273 (1995).
61. M. Wiesner *et al*., Conditional immortalization of human B cells by CD40 ligation. *PLoS One* **3**, e1464 (2008).
62. F. J. M. van Kuppeveld *et al*., Genus- and species-specific identification of mycoplasmas by 16S rRNA amplification. *Appl. Environ. Microbiol.* **58**, 2606–2615 (1992).
63. G. Miller, J. Robinson, L. Heston, M. Lipman, Differences between laboratory strains of Epstein-Barr virus based on immortalization, abortive infection, and interference. *Proc. Natl. Acad. Sci. U.S.A.* **71**, 4006–4010 (1974).
64. H. J. Delecluse, T. Hilsendegen, D. Pich, R. Zeidler, W. Hammerschmidt, Propagation and recovery of intact, infectious Epstein-Barr virus from prokaryotic to human cells. *Proc. Natl. Acad. Sci. U.S.A.* **95**, 8245–8250 (1998).
65. S. M. Yoo *et al*., Centrifugal enhancement of Kaposi's sarcoma-associated virus infection of human endothelial cells in vitro. *J. Virol. Methods* **154**, 160–166 (2008).
66. A. Nanbo, A. Sugden, B. Sugden, The coupling of synthesis and partitioning of EBV's plasmid replicon is revealed in live cells. *EMBO J.* **26**, 4252–4262 (2007).
67. J. J. Russo *et al*., Nucleotide sequence of the Kaposi sarcoma-associated herpesvirus (HHV8). *Proc. Natl. Acad. Sci. U.S.A.* **93**, 14862–14867 (1996).
68. A. Dobin *et al*., STAR: Ultrafast universal RNA-seq aligner. *Bioinformatics* **29**, 15–21 (2013).
69. Y. Liao, G. K. Smyth, W. Shi, featureCounts: An efficient general purpose program for assigning sequence reads to genomic features. *Bioinformatics* **30**, 923–930 (2014).
70. M. I. Love, W. Huber, S. Anders, Moderated estimation of fold change and dispersion for RNA-seq data with DESeq2. *Genome Biol.* **15**, 550 (2014).
71. A. Zhu, J. G. Ibrahim, M. I. Love, Heavy-tailed prior distributions for sequence count data: Removing the noise and preserving large differences. *Bioinformatics* **35**, 2084–2092 (2019).
72. A. Subramanian *et al*., Gene set enrichment analysis: A knowledge-based approach for interpreting genome-wide expression profiles. *Proc. Natl. Acad. Sci. U.S.A.* **102**, 15545–15550 (2005).
73. V. K. Mootha *et al*., PGC-1α-responsive genes involved in oxidative phosphorylation are coordinately downregulated in human diabetes. *Nat. Genet.* **34**, 267–273 (2003).
74. A. Liberzon *et al*., The Molecular Signatures Database (MSigDB) hallmark gene set collection. *Cell Syst.* **1**, 417–425 (2015).
75. D. A. Bolotin *et al*., MiXCR: Software for comprehensive adaptive immunity profiling. *Nat. Methods* **12**, 380–381 (2015).